C h a p t e r 2

PARAMAGNETIC RESONANCE SIGNALS

2.1 Introduction

The "atomic" resonance which is the basis for the proposed solid-state atomic frequency standard is the divalent vanadium ion substituted into a magnesium oxide lattice. The physics of paramagnetic defects in solids is a large topic within the subject of electron spin resonance (ESR), also called paramagnetic resonance (EPR) [1,2,3,4,5]. Paramagnetic resonance is similar to nuclear magnetic resonance, in that it involves magnetic dipole transitions between spin states, but in paramagnetic resonance the interaction is with the spin of unpaired electrons rather than the spin of the nucleus. The most useful introduction to solid-state paramagnetic resonance of transition ions is the book by J. R. Pilbrow (1990) [1]. A good general introduction to electron spin resonance is the book by Wertz and Bolton (1986) [2]. Professional references include an up-to-date handbook by Poole and Farach (1999) [3], the classic treatise on experimental techniques by Poole (1983) [4], and the classic theory of transition metal paramagnetic resonance by Abragam and Bleaney (1970) [5].

The vast majority of electron spin resonance experiments are "field-swept" or "high-field" experiments, meaning that the microwave spectrometer used to detection paramagnetic resonance operates at a fixed frequency (most commonly X-band), and a large magnetic field is applied to the sample to measure the paramagnetic absorption as a function of magnetic field. Much less common is "zero-field" and "frequency-swept" electron spin resonance, where the applied magnetic field is zero and the microwave frequency is varied. The most important articles on zero-field electron spin resonance are Delfts and Bramley (1997) [6,7], Bramley and Strach (1985) [8], and a review article Bramley and Strach (1983) [9]. An older example of zero-field measurements is reference [10], T. Cole *et al.*,

and reports the zero-field spectrum of Cr^{3+} (which has the same electronic structure as V^{++}) in magnesium oxide.

2.2 Characteristics of Transition Metal Paramagnetic Resonance in Solids

Transition metal ions are some of the most important examples of paramagnetic resonance, and magnetism in general, because the unpaired spins of the *d*-shell electrons result in magnetic properties of many transition metal compounds. For isolated transition metal ions substituting into a diamagnetic crystal lattice, the electronic energy levels are very different from the free ion because of the electric field of the neighboring cations (*i.e.*, ligand fields.) The ligand fields lift the degeneracy of the *d*-shell, and the resulting energy splitting results in the colors characteristic of transition metal complexes. The specifics of the crystal field splitting strongly depend on the lattice symmetry, which is described in the literature [1, 2, 5].

The spin of the *d*-shell electrons interacts with the crystal lattice via spin-orbit coupling, which depends on the orbital angular momentum of the *d*-electrons in the crystal. Generally, the orbital angular momentum in a crystal lattice is not the same as the orbital angular momentum of the free ion. When the spin-orbit coupling is zero, the electron spin states usually have a long relaxation lifetime and the paramagnetic resonance spectrum can be measured at *room temperature*. For example, in a cubic crystal, ions with the electronic structure $3d^3$ (*e.g.*, V^{++}, Cr^{3+}) and $3d^5$ (*e.g.*, Mn^{++}) have orbitally non-degenerate ground states. An orbitally non-degenerate ground state must have zero orbital angular momentum and therefore the spin-orbit coupling is close to zero ([2], p. 263). The result is that the paramagnetic resonance spectrum of these ions in cubic lattices is easily observed at room temperature. The details of thermal relaxation can be complex at low temperature, where concentration depend interactions between the paramagnetic species may be important (*e.g.*, [11]). However, at room temperature, the picture of a single ion interacting with the crystal lattice is usually accurate.

For future reference, the temperature dependence of the paramagnetic resonance spectrum of certain ions in various crystal lattices has been studied, as reported in [12]. In general, ionic crystals have the least temperature dependence, whereas more covalent crystals have stronger temperature dependence because of the partial bonding between the *d*-electrons and surrounding ligands.

2.3 Zero-Field Electron Spin Resonance of Vanadium in Magnesium Oxide

The remainder of the chapter develops the specific quantum mechanics needed to describe the zero-field paramagnetic resonance spectrum of divalent vanadium in cubic symmetry, or similar ions where the spin Hamiltonian is given by an isotropic hyperfine interaction. In general, there are many possible choices of ions, which may have anisotropic hyperfine terms and non-zero crystal field terms in the spin Hamiltonian; however, we will show for the example of vanadium some of the interesting features of zero-field paramagnetic resonance such as the existence of narrow magnetic field independent transitions which are insensitive to dipolar broadening. The theory of dipolar broadening and concentration dependence is developed in Chapter 3.

The specific results calculated below describe the frequency, intensity, polarization, and Zeeman shift of the zero-field paramagnetic resonance of divalent vanadium in magnesium oxide. The details are different from the high-field approximation used in most electron spin resonance measurements, because the eigenstates at zero-field are those of the coupled basis F, defined in Section 2.5, rather than eigenfunctions of the electron spin angular momentum operator $\mathbf{S}$. The analysis at zero-field is mathematically the same as results for spin-orbit coupling used in atomic physics [13]. The later sections of the chapter also calculate the magnetic susceptibility of a paramagnetic sample and the effect on the frequency and losses of an electrical resonator containing the sample. Finally, several examples of numerically calculated spectra and example measurements are given.

2.4 Hamiltonian for V^{++} in a Cubic Lattice

The spin resonance of divalent vanadium results from three unpaired electrons in the *d*-shell ($3d^3$). The spin of the electrons ($S = 3/2$) couples to the spin of the nucleus ($I = 7/2$) via the hyperfine interaction. In the most general case, the spin Hamiltonian for divalent vanadium in a cubic crystal lattice with eight equivalent directions, *i.e.*, in octahedral symmetry, is ([5], *c.f.*, Chapter 18):

$$\begin{aligned} \mathrm{H} &= g\beta\mathbf{S}\cdot\mathbf{H} + A\mathbf{S}\cdot\mathbf{I} + u\beta[\mathbf{S}_x^3 H_x + \mathbf{S}_y^3 H_y + \mathbf{S}_z^3 H_z - \frac{1}{5}(\mathbf{S}\cdot\mathbf{H})\{3S(S+1)-1\}] \\ &+ U[\mathbf{S}_x^3 I_x + \mathbf{S}_y^3 I_y + \mathbf{S}_z^3 I_z - \frac{1}{5}(\mathbf{S}\cdot\mathbf{I})\{3S(S+1)-1\}] \end{aligned} \tag{2.1}$$

The first term is the Zeeman interaction between the magnetic moment of the electrons $g\beta\mathbf{S}$ and an applied magnetic field **H**. The factor *g* is called the electron *g*-factor, and is usually close to 2 for ions with room temperature spectra [1,2]. The g-factor for the electron spin is 1.98 for vanadium in magnesium oxide [14]. The factor β is the Bohr magneton, and equals 1.4 *MHz / Gauss* using frequency units rather than energy. The second term is the isotropic hyperfine interaction between the nuclear spin, represented by the angular momentum operator **I**, and the electron spin, represented by the angular momentum operator **S**. The hyperfine constant has been determined from high-field measurements, and is approximately 223 *MHz*, again using frequency rather than energy units [12,14,15]. The parameter *u* in Equation 2.1 has been measured in the isoelectronic Cr^{3+}/MgO system, which determined $u = 10^{-4}$ at 300 K [16]. Hence, the terms in *u* are much smaller than the isotropic Zeeman term proportional to $g \sim 2$. Similarly, the coefficient *U* is expected to be much smaller than the hyperfine coupling *A*. (In principle, higher order quadropole interactions may exist which are not shown in the spin Hamiltonian (2.1), and may add non-zero terms even in cubic symmetry [17,18]. These higher order quadropole interactions

are expected to be very small.) Considering the higher order terms proportional to u and U as perturbations, the Hamiltonian is simply:

$$\mathrm{H} = g\beta\mathbf{S}\cdot\mathbf{H} + A\mathbf{S}\cdot\mathbf{I} \tag{2.2}$$

The vanadium spin Hamiltonian (2.2) is similar to the spin Hamiltonian which describes the hyperfine interaction for the valence electron of an alkali metal occupying an *S*-orbital (*i.e.*, an orbital with zero orbital angular momentum). Several important results, such as the existence of magnetic field independent allowed transitions, are features of the spin Hamiltonian (2.2).

2.5 Magnetic Resonance at Zero-Field

The eigenvalues of (2.2) at zero-field can be easily calculated in the coupled basis *F*. The angular momentum operator **F** is defined as the sum of the electronic angular momentum operator **S** and the nuclear spin operator **I**:

$$\mathbf{F} = \mathbf{I} + \mathbf{S} \tag{2.3}$$

The "coupled basis" is defined by the simultaneous eigenfunctions of the angular momentum operators $\mathbf{F}^2$, $\mathbf{I}^2$, $\mathbf{S}^2$, and $\mathbf{F}_z$. The scalar hyperfine term is diagonal in the coupled basis, as shown below:

$$\mathbf{F}^2 = (\mathbf{I}+\mathbf{S})^2 = \mathbf{I}^2 + 2\mathbf{I}\cdot\mathbf{S} + \mathbf{S}^2 \tag{2.4}$$

$$\Rightarrow \mathbf{I}\cdot\mathbf{S} = \frac{1}{2}\left(\mathbf{F}^2 - \mathbf{I}^2 - \mathbf{S}^2\right) \tag{2.5}$$

Hence, because $\mathbf{F}^2$, $\mathbf{I}^2$, and $\mathbf{S}^2$ are diagonal in the coupled basis, the matrix representing $\mathbf{I}\cdot\mathbf{S}$ is also diagonal, with eigenvalues:

$$\mathbf{I}\cdot\mathbf{S}\left|F, m_F\right\rangle = \frac{1}{2}\left[F(F+1) - S(S+1) - I(I+1)\right]\left|F, m_F\right\rangle \tag{2.6}$$

The allowed values for F are from $I + S$ to $|I - S|$ in integer steps. For example, for divalent vanadium ($I = 7/2$, $S = 3/2$), F takes the values 5, 4, 3, and 2, as shown in Table 2.1. The corresponding energies are calculated using Equation 2.6. There are $2F + 1$ degenerate eigenvalues for each value of F, which is summarized in Table 2.1.

F	Energy	Degeneracy
5	$\frac{21}{4}A$	11
4	$\frac{1}{4}A$	9
3	$-\frac{15}{4}A$	7
2	$-\frac{27}{4}A$	5

Table 2.1: Zero-Field Hyperfine Energy Levels

As will be described in greater detail in Section 2.6, zero-field magnetic resonance transitions obey the selection rule $\Delta F = \pm 1$, which corresponds to transitions with frequencies 5A, 4A, 3A for the vanadium system. The result for the transition energies is also called the Landé interval rule. Therefore, the zero-field magnetic resonance spectrum of vanadium has three resonance lines, with transition frequencies of approximately 669 MHz, 892 MHz, and 1115 MHz.

The effect of a static magnetic field, represented by the first term in Equation 2.2, is to lift the degeneracy of each F manifold. If the external magnetic field is small compared to the hyperfine interaction, then the first-order perturbation to the transition frequencies is calculated from the diagonal elements of the operator $\mathbf{S}_z$ represented in the coupled basis.

Generally, the representation of an angular momentum operator **S** in the coupled basis will be a product of one factor which depends only on the quantum number F, and a second factor involving both F and m_F. The complete calculation of the matrix representing an angular momentum operator in the coupled basis is detailed in Condon & Shortley [13].

For example, the diagonal elements of $\mathbf{S}_z$ are:

$$\left\langle F, m_F \left| g_S \frac{\mu_B}{\hbar} \mathbf{S}_Z \right| F, m_F \right\rangle = g_F \frac{\mu_B}{\hbar} \hbar m_F \tag{2.7}$$

where g_F is called the Landé g-factor, equal to:

$$g_F = g_S \left[\frac{F(F+1) + S(S+1) - I(I+1)}{2F(F+1)} \right] \tag{2.8}$$

For $S = 3/2$ and $I = 7/2$, the Landé g-factor is

$$g_F = g_S \left[\frac{F(F+1) - 12)}{2F(F+1)} \right] \tag{2.9}$$

The Landé factors for the F-states of V^{++} are shown in Table 2.2 below.

F	g_F-factor	$F(F+1)$	$F(F+1)g_F^2$
5	$\frac{3}{10}g_S$	30	$\frac{27}{10}g_S^2$
4	$\frac{2}{10}g_S$	20	$\frac{8}{10}g_S^2$
3	0	12	0
2	$-\frac{1}{2}g_S$	6	$\frac{15}{10}g_S^2$

Table 2.2: Landé factors to calculate Zeeman shift for the F-states of V^{++}

The Zeeman shift of a resonance line is determined by the difference of the Landé factors and quantum numbers m_F of the initial and final states. There are $2F + 1$ Zeeman levels in each F manifold corresponding to the eigenvalues $m_F = \{F, F - 1, F - 2, \ldots, -|F - 1|, -F\}$. The Zeeman shift for each set of F sublevels of V^{++}/MgO is plotted in Figure 2.1:

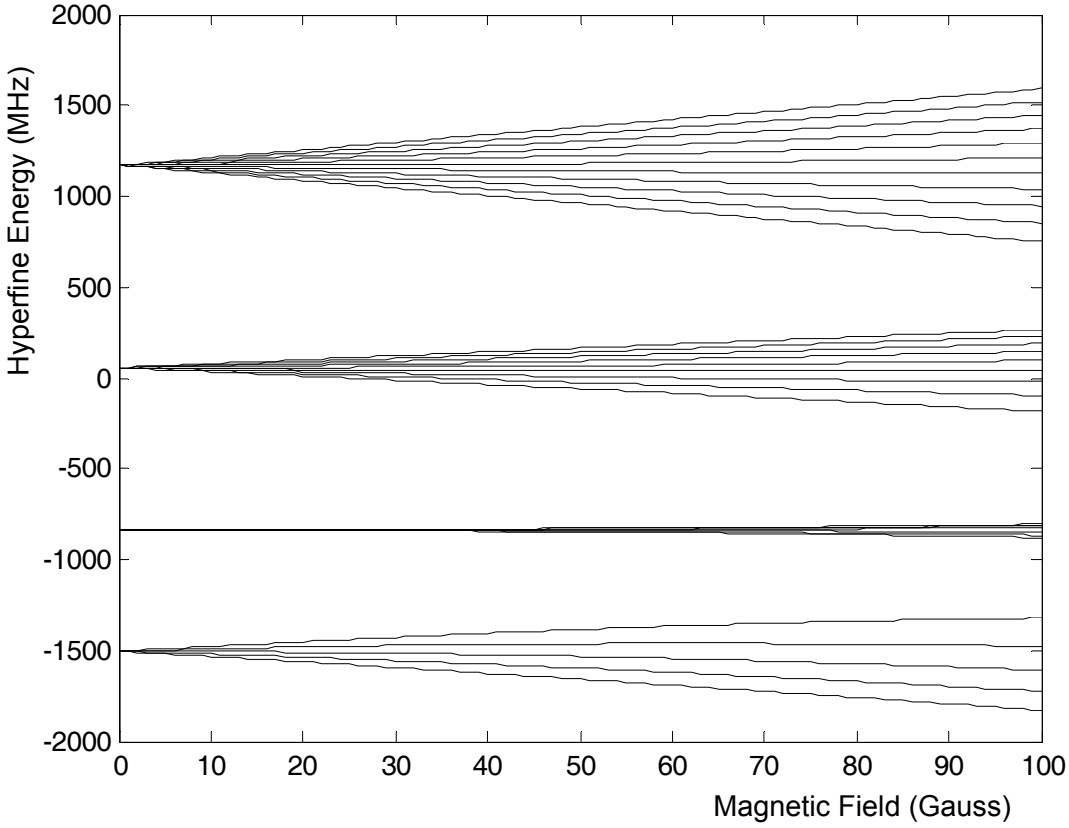

Figure 2.1: Numerically Calculated Zeeman Shift for V++/MgO

In the figure, the exact eigenvalues are used from a numerical solution to Equation 2.2 at each value of the applied magnetic field **H**. The second-order Zeeman shift is evident at magnetic fields above approximately 50 Gauss. For Zeeman fields from 0 to 20 Gauss, the first-order theory is a close approximation to the exact solution.

2.6 Selection Rules for Parallel and Perpendicular Polarizations

The selection rules and Zeeman shift for transitions between the F-levels can be explicitly calculated. In the following, the direction of the Zeeman field is chosen to define the z-axis. The intensities of the allowed transitions are simply given by the square of the non-zero off-diagonal elements of the operators $\mathbf{S}_x$ and $\mathbf{S}_z$ represented in the coupled basis. The intensities of z-polarized transitions, which are non-zero for transitions from F to $F \pm 1$, and between states with the same quantum number m_F, are {Condon & Shortley § 9^3(11) and § 10^3(5), [13]}:

$$\left\langle F, m_F \left| S_z \right| F-1, m_F \right\rangle^2 = \frac{\left[F^2-(S-I)^2\right]\left[(S+I+1)^2-F^2\right]}{4F^2(4F^2-1)}\hbar^2\left(F^2-m_F^2\right) \qquad (2.10)$$

The transitions with radio-frequency field perpendicular to the Zeeman field, the intensities are proportional to:

$$\left\langle F, m_F \left| S_x \right| F-1, m_F \pm 1 \right\rangle^2 = \frac{\left[F^2-(S-I)^2\right]\left[(S+I+1)^2-F^2\right]}{4F^2(4F^2-1)}\hbar^2\frac{1}{4}\left(F \mp m_F\right)\left(F \mp m_F - 1\right) \qquad (2.11)$$

Allowed transitions for perpendicular polarization obey the selection rules: F to $F \pm 1$, and m_F to $m_F \pm 1$. Notice the selection rule for m_F is different for parallel and perpendicular polarizations. The intensities Equations (2.10) and (2.11) are tabulated in Tables 2.3 and 2.4 at the end of this Chapter.

The relative transition intensities are plotted for both polarizations in Figure. 2.2 below:

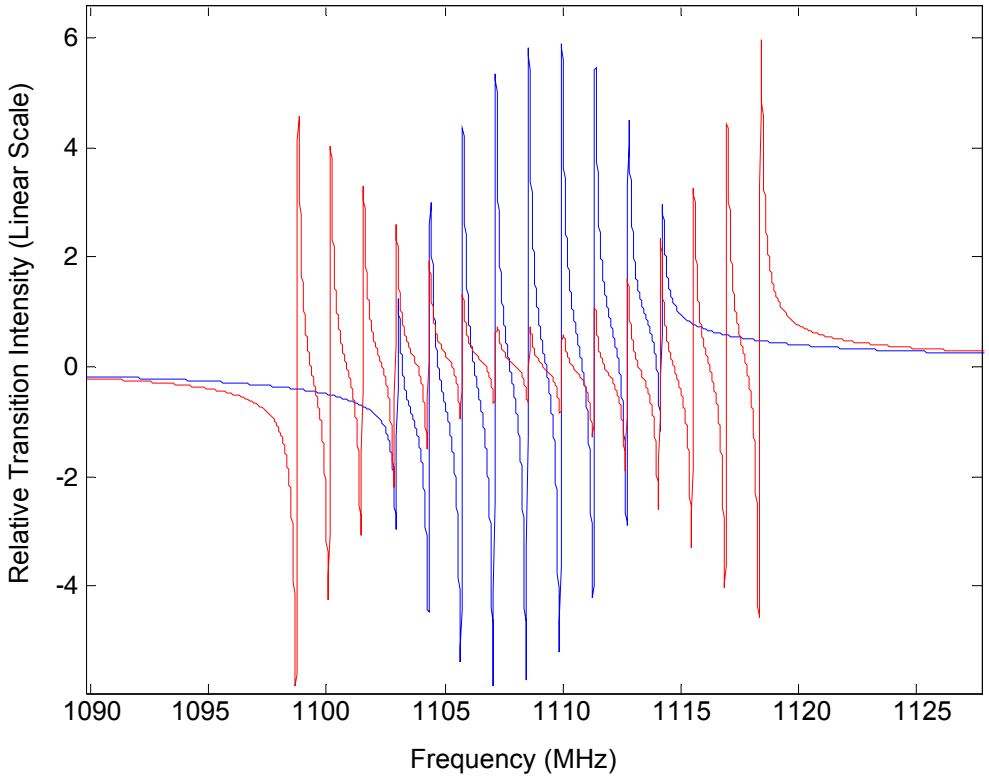

Figure 2.2: Transition Intensities for Parallel and Perpendicular Polarizations

The figure uses a numerical solution of Equation (2.2), and assumes that all transition have the same Lorentzian dispersion lineshape and resonance width. The Zeeman field is 10 Gauss in Figure 2.2. The difference between *z* (blue) and *x* (red) polarized intensities allows a measurement of the spectrum by modulating the polarization of the magnetic field which defines the quantization axis (or equivalently, the relative polarization of the RF field). The difference between *x*- and *z*- polarized transitions at low-field can be used to measure the the $m_F = 0$ to $m_F = 0$ magnetic field independent transition without using a large (100 Gauss or more) modulation field.

Of course, the intensity at zero-field cannot have a polarization, *i.e.*, the sum over all *x*-polarized transition intensities is the same as the sum over all *z*-polarized transitions.

2.7 Magnetic Susceptibility

This section calculates the resonant magnetic susceptibility due to magnetic resonance transitions of the type described in Section (4).

The transition rate between the zero-field hyperfine levels is given by (c.f. Yariv, 1967 ref. [2]):

$$W_{m\to k} = \frac{1}{\hbar^2}\left|H'_{km}\right|^2 g(\nu) \tag{2.12}$$

where g(ν) is a normalized lineshape function:

$$\int_{-\infty}^{\infty} g(\nu_k)\,d\nu_k = 1 \tag{2.13}$$

The transition rate for the *z*-polarized $F = 5$ to $F = 4$ magnetic field independent transition is:

$$W_{m\to k} = \frac{5775}{99000}\left(\frac{g_S\mu_B}{\hbar}H_{z,RF}\right)^2 g(\nu) = 0.0583\omega_1^2 g(\nu) \tag{2.14}$$

where $H_{z,RF}$ is the magnitude of the RF magnetic field. The magnetic susceptibility is (Yariv 1967, (8.2-2) [2]):

$$\chi''(\upsilon) = 0.0583\cdot 2\hbar\left(\frac{g_S\mu_B}{\hbar}\right)^2 g(\nu)\left[N_{F=5,M=0} - N_{F=4,M=0}\right] \tag{2.15}$$

The thermal population difference is

$$N_{F=5,M=0} - N_{F=4,M=0} \cong \frac{1}{32}\frac{\hbar 2\pi\nu_0}{kT}N \tag{2.16}$$

where N is the density of paramagnetic ions and ν_0 is the resonant frequency. Suppose the g(ν) is Lorentzian with "half-power" width of Δν:

$$g(v-v_0)=\frac{\Delta v}{2\pi[(v-v_0)^2+(\Delta v/2)^2]} \tag{2.17}$$

$$g\ (\ 0\ )\ =\ \frac{2}{\pi\ \Delta\ v} \tag{2.18}$$

Therefore, the magnetic susceptibility due to the *z*-polarized 0-0 transition is:

$$\chi''(\upsilon_0)=0.0583\cdot 2\hbar\left(\frac{g_S\mu_B}{\hbar}\right)^2\frac{\Delta v}{2\pi[(v-v_0)^2+(\Delta v/2)^2]}\frac{1}{32}\frac{\hbar 2\pi\nu_0}{kT}N \tag{2.19}$$

$$\chi''(\upsilon_0)=0.0583\cdot\frac{1}{16}\frac{(g_S\mu_B)^2}{kT}\frac{\Delta v\nu_0}{[(v-v_0)^2+(\Delta v/2)^2]}N \tag{2.20}$$

As an example, we calculate the resonant magnetic susceptibility for a magnesium oxide crystal doped with 100 ppm vanadium relative to the anion lattice. The concentration of spin is:

$$N=\frac{3.58\,g/cc}{16+24.3\,g/mol}\times 100\,ppm\times(6.022\times10^{23}\,mol^{-1})=5.35\times10^{18}/cc \tag{2.21}$$

The physical constants are (in CGS units):

$$\frac{(g_S\mu_B)^2}{kT}=\frac{(2\cdot 9.264\times10^{-21}\,ergG^{-1})^2}{(1.38\times10^{-16}\,ergK^{-1})\cdot 300K}=8.29\times10^{-27}\,ergG^{-2} \tag{2.22}$$

$$\chi''(\upsilon_0)=0.0583\cdot\frac{1}{16}8.29\times10^{-27}\,ergG^{-2}\frac{\Delta v\nu_0}{[(v-v_0)^2+(\Delta v/2)^2]}5.35\times10^{18}/cc \tag{2.23}$$

The numerical expression for the magnetic susceptibility is:

$$\chi''(\upsilon_0) = 1.62 \times 10^{-10} ergG^{-2} cc^{-1} \frac{\Delta v \nu_0}{[(v - \nu_0)^2 + (\Delta v / 2)^2]} \tag{2.24}$$

Converting to MKS units, the equivalent magnetic susceptibility is:

$$4\pi\chi''(\upsilon_0) = 2.04 \times 10^{-9} \frac{\Delta v \nu_0}{[(v - \nu_0)^2 + (\Delta v / 2)^2]} \tag{2.25}$$

which for a 5 MHz wide resonance at 1110 MHz is equal to 1.81×10^{-6}.

The total zero-field intensity for 5 MHz and 100 ppm is $6.6*1.81 = 1.2 \times 10^{-5}$.

2.8 Circuit Model for Electrical Resonator Containing Paramagnetic Sample

.

A model for an electrical resonator containing a paramagnetic sample is now easily developed using the magnetic susceptibility. The effective inductance of the loop-gap resonator or other resonator containing the paramagnetic sample is modified by the change in magnetic susceptibility:

$$L = L_0(1 + 4\pi\eta\chi) \tag{2.26}$$

The fill factor is equal to:

$$\eta = \frac{\int_{sample} H_1^2 dv}{\int_{cavity} H_1^2 dv} \tag{2.27}$$

In the present experiment, the fill factor is approximately 1/3.

(ii) Calculate the frequency modulation of the resonator due to paramagnetic sample

The resonant frequency is:

$$(2\pi\nu_0)^2 = \frac{1}{LC} \tag{2.28}$$

and for a small change in inductance, the frequency perturbation is:

$$\frac{\partial \nu_0}{\nu_0} = -\frac{1}{2}\frac{\partial L}{L} = -\frac{1}{2}4\pi\eta\chi \tag{2.29}$$

(iii) Calculate the resonator frequency modulation introduced phase modulation to the transmitted carrier. The electrical resonator dispersion at resonance is:

$$\frac{\partial \theta}{\partial \nu_0} = \frac{2Q_L}{\nu_0} \tag{2.30}$$

The phase-modulation introduced by the paramagnetic resonance is therefore

$$\partial\theta = -4\pi\eta Q_L \chi \tag{2.31}$$

The single-sideband power due to phase modulation is:

$$P = 20\log 4\pi\eta Q_L \chi_{RMS} \tag{2.32}$$

For example, if the fill factor is 1/3 and the loaded-Q is 250, the sideband power due to 5 MHz wide transition with intensity of Z, 0-0, is -76 dBc.

(iv) Calculate the sensitivity assuming thermal noise limit

The thermal noise power kT is equal to -174 dBm. If the receiver has a 3dB noise figure, the noise floor is -171 dBm. The theoretical sensitivity is therefore 95 dB from a 0dBm carrier.

2.9 Numerical Calculation of Eigenvalues and Transition Intensities

Another very useful technique is to numerically solve for the eigenvalues and energies of the spin Hamiltonian, then plot the spectrum by generating a matrix with the frequencies and intensities of the magnetic dipole transitions. An example shown below is the spectrum of Mn^{++} ion at zero field, which is more complex that the V^{++} spectrum because of the non-zero crystal field terms in the spin Hamiltonian for S = 5/2 in cubic symmetry. The spectrum is calculated using published values for the hyperfine interaction and crystal field term determined from high-field measurements [13,14].

The zero-field magnetic resonance measurements presented in this thesis measure the dispersion introduced by the paramagnetic resonance of the sample (*i.e.*, the real component of the magnetic susceptibility), rather than measuring absorption (*i.e.*, the imaginary component of the magnetic susceptibility.) When comparing experimental results to calculation, the spectrum assumes Lorentzian dispersion lineshapes for all transitions, modeled using the function:

$$g(\nu-\nu_0)=\frac{\Delta\nu(\nu-\nu_0)}{2\pi[(\nu-\nu_0)^2+(\Delta\nu/2)^2]} \tag{2.33}$$

The measured spectrum is the difference between the dispersive component of the magnetic susceptibility at zero magnetic field and the dispersive component of the magnetic susceptibility at the peak Zeeman modulation field. These aspects of the magnetic resonance measurement are detailed in Chapter 4.

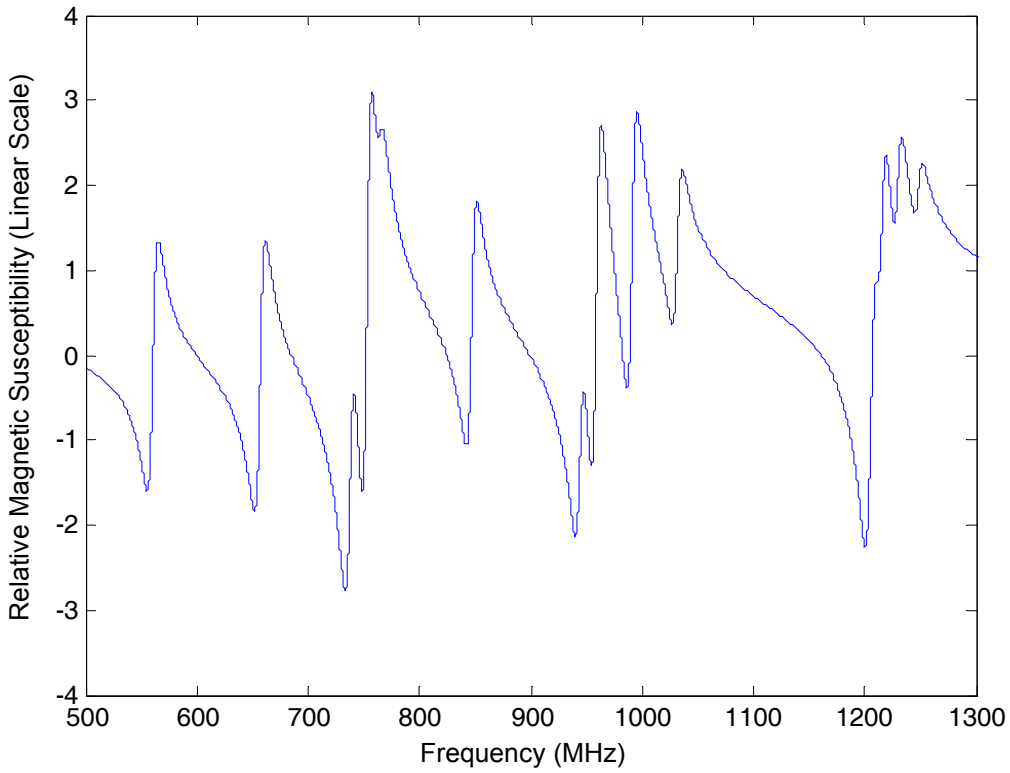

Figure 2.3: Calculated Spectrum for Mn^{++} in Magnesium Oxide

A typical calculation is shown in Figure 2.3 above, calculated using the published parameters for the spin Hamiltonian of Mn^{++}/MgO. The numerical model does not account for the variations in dipolar resonance widths, discussed in Chapter 3. The spectrum shows that Mn^{++} ions in a magnesium oxide sample have zero-field paramagnetic resonance signals in the range of 500 to 1300 MHz.

An example of a calculated dispersion spectrum of a sample containing both manganese and vanadium in MgO is shown in Figure 2.4 below, assuming all transitions have the same 10 MHz linewidth:

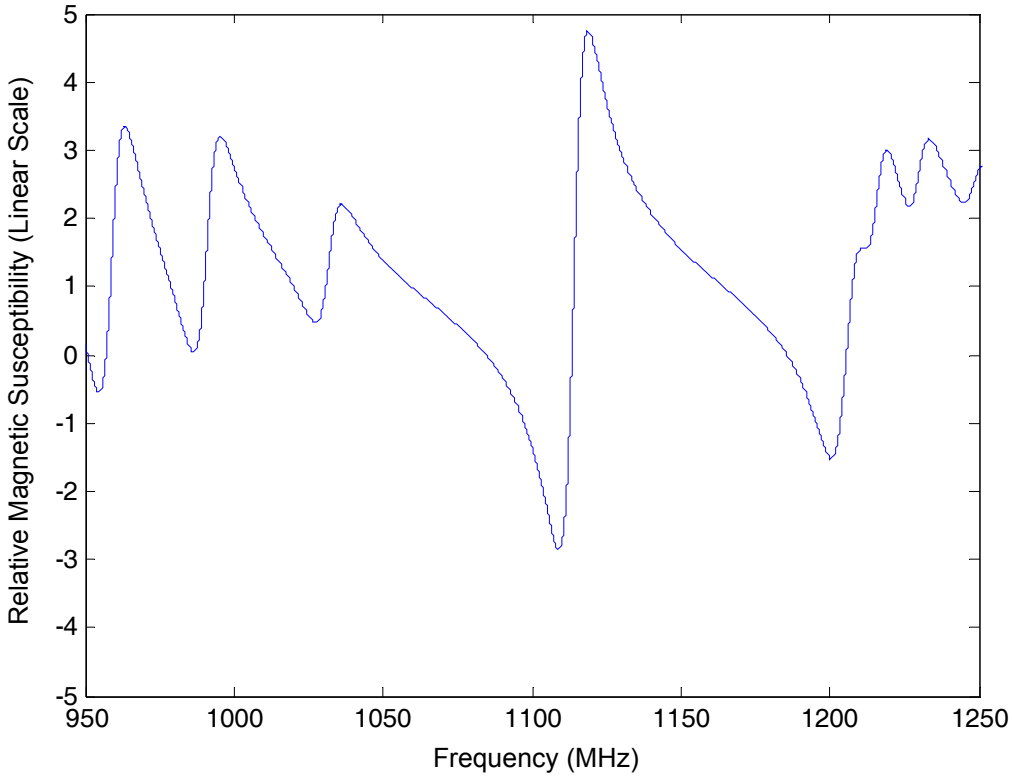

Figure 2.4: Example Calculated Spectrum for Mn^{++} and V^{++} in Magnesium Oxide

The large resonance at 1115 MHz is due to the highest frequency zero-field transitions of V++/MgO, and the remaining signals in the 1000 to 1200 MHz range are due to manganese ions.

2.10 Comparison to Measurement

A *measured* zero-field paramagnetic spectrum of a sample of magnesium oxide containing both vanadium and manganese is shown below in Figure 2.5. The modulation field was approximately 12 Gauss. Details of the zero-field spectrometer design are described in Chapter 4. The red curve is the measured spectrum and the blue curve is a calculation. We can see that the basic features of the calculated and measured spectrum are the same. The zero-field measurement allows for a more precise determination of the hyperfine coupling which is seen to be approximately 1% lower than the published value determined from high-field measurements [14].

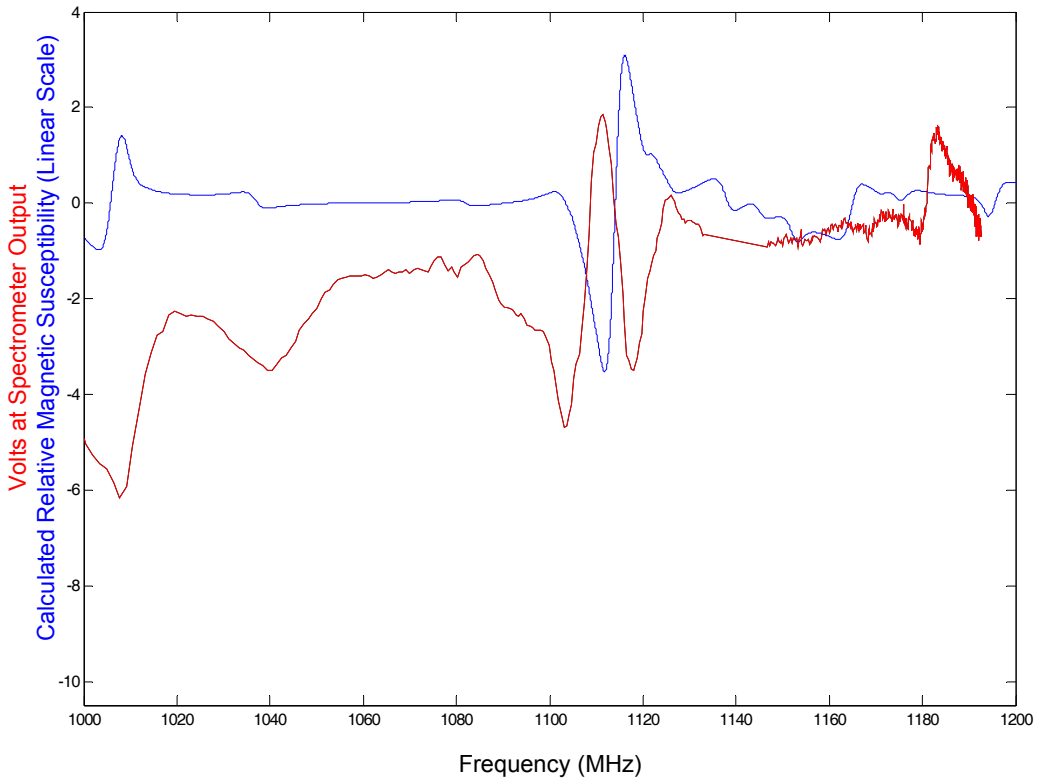

Figure 2.5: Measured Spectrum for Mn^{++} and V^{++} in Magnesium Oxide

The measured curve is the output in volts from the zero-field magnetic resonance spectrometer described in Chapter 4. The blue curve was calculated similar to Figure 2.4, using published parameters for V^{++} and Mn^{++} ions in magnesium oxide known from high-field measurements. The relative intensities of the vanadium and manganese spectrum, as well as the resonance widths, were adjusted to approximately match the measured spectrum. Therefore, the measurement in Figure 2.5 validates the model of zero-field magnetic resonance presented in this chapter. Chapter 3 will discuss the linewidths at zero-field in greater detail.

Table 2.3: Transition Intensities and Zeeman Shift for Parallel Polarization between F = 4 and F = 5 States

Transition $\lvert F,m_F\rangle$	F only factor	F and m_F factor	Intensity	Zeeman Shift
|5,4> -> |4,4>	$\frac{231}{99000}\hbar^2$	9	$\frac{2079}{99000}\hbar^2$	$\frac{4}{10}g_S\hbar$
|5,3> -> |4,3>	$\frac{231}{99000}\hbar^2$	16	$\frac{3696}{99000}\hbar^2$	$\frac{3}{10}g_S\hbar$
|5,2> -> |4,2>	$\frac{231}{99000}\hbar^2$	21	$\frac{4851}{99000}\hbar^2$	$\frac{2}{10}g_S\hbar$
|5,1> -> |4,1>	$\frac{231}{99000}\hbar^2$	24	$\frac{5544}{99000}\hbar^2$	$\frac{1}{10}g_S\hbar$
|5,0> -> |4,0>	$\frac{231}{99000}\hbar^2$	25	$\frac{5775}{99000}\hbar^2$	0
|5,-1> -> |4,-1>	$\frac{231}{99000}\hbar^2$	24	$\frac{5544}{99000}\hbar^2$	$-\frac{1}{10}g_S\hbar$
|5,-2> -> |4,-2>	$\frac{231}{99000}\hbar^2$	21	$\frac{4851}{99000}\hbar^2$	$-\frac{2}{10}g_S\hbar$
|5,-3> -> |4,-3>	$\frac{231}{99000}\hbar^2$	16	$\frac{3696}{99000}\hbar^2$	$-\frac{3}{10}g_S\hbar$
|5,-4> -> |4,-4>	$\frac{231}{99000}\hbar^2$	9	$\frac{2079}{99000}\hbar^2$	$-\frac{4}{10}g_S\hbar$
Total	$\frac{231}{99000}\hbar^2$	165	$\frac{38115}{99000}\hbar^2$	

Table 2.4: F = 5 to F = 4 Transition Intensities and Zeeman Shift for Perpendicular Polarization.

The table calculates the overall intensity for the 15 non-degenerate transitions resolved via the Zeeman shift. In general, more than one allowed transition contributes to each line in the Zeeman spectrum for perpendicular polarization.

Transition $\lvert F,m_F\rangle$	F only factor	F and m_F factor	Intensity	Zeeman Shift
$\lvert 5,5\rangle \leftrightarrow \lvert 4,4\rangle$	$\frac{231}{99000}\hbar^2$	$\frac{90}{4}$	$\frac{5198}{99000}\hbar^2$	$\frac{7}{10}g_S\hbar$
$\lvert 5,4\rangle \leftrightarrow \lvert 4,3\rangle$	$\frac{231}{99000}\hbar^2$	$\frac{72}{4}$	$\frac{4158}{99000}\hbar^2$	$\frac{6}{10}g_S\hbar$
$\lvert 5,3\rangle \leftrightarrow \lvert 4,2\rangle$	$\frac{231}{99000}\hbar^2$	$\frac{56}{4}$	$\frac{3234}{99000}\hbar^2$	$\frac{5}{10}g_S\hbar$
$\lvert 5,2\rangle \leftrightarrow \lvert 4,1\rangle$	$\frac{231}{99000}\hbar^2$	$\frac{42}{4}$	$\frac{2426}{99000}\hbar^2$	$\frac{4}{10}g_S\hbar$
$\lvert 5,1\rangle \leftrightarrow \lvert 4,0\rangle$	$\frac{231}{99000}\hbar^2$	$\frac{30}{4}$	$\frac{1733}{99000}\hbar^2$	$\frac{3}{10}g_S\hbar$
$\lvert 5,0\rangle \leftrightarrow \lvert 4,-1\rangle$	$\frac{231}{99000}\hbar^2$	$\frac{20}{4}$	$\frac{1155}{99000}\hbar^2$	$\frac{2}{10}g_S\hbar$
$\lvert 5,3\rangle \leftrightarrow \lvert 4,4\rangle$	$\frac{231}{99000}\hbar^2$	$\frac{2}{4}$	$\frac{116}{99000}\hbar^2$	$\frac{1}{10}g_S\hbar$
$\lvert 5,-1\rangle \leftrightarrow \lvert 4,-2\rangle$	$\frac{231}{99000}\hbar^2$	$\frac{12}{4}$	$\frac{693}{99000}\hbar^2$	$\frac{1}{10}g_S\hbar$
$\lvert 5,2\rangle \leftrightarrow \lvert 4,3\rangle$	$\frac{231}{99000}\hbar^2$	$\frac{6}{4}$	$\frac{347}{99000}\hbar^2$	0
$\lvert 5,-2\rangle \leftrightarrow \lvert 4,-3\rangle$	$\frac{231}{99000}\hbar^2$	$\frac{6}{4}$	$\frac{347}{99000}\hbar^2$	0
$\lvert 5,1\rangle \leftrightarrow \lvert 4,2\rangle$	$\frac{231}{99000}\hbar^2$	$\frac{12}{4}$	$\frac{693}{99000}\hbar^2$	$-\frac{1}{10}g_S\hbar$
$\lvert 5,-3\rangle \leftrightarrow \lvert 4,-4\rangle$	$\frac{231}{99000}\hbar^2$	$\frac{2}{4}$	$\frac{116}{99000}\hbar^2$	$-\frac{1}{10}g_S\hbar$
$\lvert 5,0\rangle \leftrightarrow \lvert 4,1\rangle$	$\frac{231}{99000}\hbar^2$	$\frac{20}{4}$	$\frac{1155}{99000}\hbar^2$	$-\frac{2}{10}g_S\hbar$

$\|5,-1\rangle \leftrightarrow \|4,0\rangle$	$\frac{231}{99000}\hbar^2$	$\frac{30}{4}$	$\frac{1733}{99000}\hbar^2$	$-\frac{3}{10}g_S\hbar$
$\|5,-2\rangle \leftrightarrow \|4,-1\rangle$	$\frac{231}{99000}\hbar^2$	$\frac{42}{4}$	$\frac{2426}{99000}\hbar^2$	$-\frac{4}{10}g_S\hbar$
$\|5,-3\rangle \leftrightarrow \|4,-2\rangle$	$\frac{231}{99000}\hbar^2$	$\frac{56}{4}$	$\frac{3234}{99000}\hbar^2$	$-\frac{5}{10}g_S\hbar$
$\|5,-4\rangle \leftrightarrow \|4,-3\rangle$	$\frac{231}{99000}\hbar^2$	$\frac{72}{4}$	$\frac{4158}{99000}\hbar^2$	$-\frac{6}{10}g_S\hbar$
$\|5,-5\rangle \leftrightarrow \|4,-4\rangle$	$\frac{231}{99000}\hbar^2$	$\frac{90}{4}$	$\frac{5198}{99000}\hbar^2$	$-\frac{7}{10}g_S\hbar$
Total	$\frac{231}{99000}\hbar^2$	165	$\frac{38115}{99000}\hbar^2$	

Notes on Table 2.4:

The Zeeman shift of a particular transition is determined by subtracting the Landé factors of the corresponding energy levels:

$$Z = g_{F=5}\mu_B m_{F=5} - g_{F=4}\mu_B m_{F=4} \tag{2.4.1}$$

There are 18 allowed transitions and 15 non-degenerate transitions.

Using the selection rules for perpendicular polarization are $\Delta F \pm 1$, $\Delta m_F \pm 1$, and the Landé factors from Table 2, we find for a transition from $F = 5$ to $F = 4$:

$$Z = \frac{3}{10}g_S\mu_B m_{F=5} - \frac{2}{10}g_S\mu_B(m_{F=5} \pm 1) = \frac{1}{10}g_S\mu_B m_{F=5} \mp \frac{2}{10}g_S\mu_B \tag{2.4.2}$$

For example, a transition from $F = 5$, $m_F = 2$ to $F = 4$, $m_F = 3$ has zero first-order Zeeman shift. The largest Zeeman is for the transition $F = 5$, $m_F = 5$ to $F = 4$, $m_F = 4$, and similarly for $F = 5$, $m_F = -5$ to $F = 4$, $m_F = -4$.

BIBLIOGRAPHY, CHAPTER 2

[1] J. R. Pilbrow, *Transition Ion Electron Paramagnetic Resonance*, Clarendon Press Oxford, 1990.

[2] J. E. Wertz and J. R. Bolton, *Electron Spin Resonance: Elementary Theory and Practical Applications*, Chapman and Hall Ltd., 1986.

[3] Charles P. Poole, Jr. and Horacia A. Farach, *Handbook of Electron Spin Resonance*, Volume 1 and 2, Springer-Verlag New York, Inc., 1999.

[4] Charles P. Poole, Jr., *Electron Spin Resonance: A Comprehensive Treatise on Experimental Techniques*, Wiley, 1983.

[5] A. Abragam and B. Bleaney, *Electron Paramagnetic Resonance of Transition Ions*, Clarendon Press, Oxford, 1970.

[6] Christopher D. Delfs and Richard Bramley, "Zero-field Electron Magnetic Resonance Spectra of Copper Carboxylates," *J. Chem. Phys.*, vol. 107, pp. 8840, 1997.

[7] Christopher D. Delfs and Richard Bramely, "The Zero-field ESR Spectrum of a Copper Dimmer," *Chemical Physics Letters*, vol. 264, pp. 333, 1997.

[8] Richard Bramley and Steven J. Strach, "Zero-Field EPR of the Vanadyl Ion in Ammonium Sulfate," *J. of Magnetic Resonance*, vol. 61, pp. 245, 1985.

[9] Richard Bramley and Steven J. Strach, "Electron Paramagnetic Resonance Spectroscopy at Zero Magnetic Field," *Chem. Rev.*, vol. 83, pp. 49-82, 1983.

[10] Cole, T. Kushida, T., and Heller, H. C., "Zero-Field Electron Magnetic Resonance in Some Inorganic and Organic Radicals," *J. Chem. Phys.*, vol. 38, pp. 2915, 1963.

[11] P. R. Solomon, "Relaxation of Mn^{2+} and Fe^{3+} Ions in Magnesium Oxide," *Phys. Rev.*, vol. 152, no. 1, December 1966.

[12] Walter M. Walsh, Jr., Jean Jeener, and N. Bloembergen, "Temperature-Dependent Crystal Field and Hyperfine Interactions," *Phys. Rev.*, vol. 139, pp. A 1338, 1965.

[13] E. U. Condon & G. H. Shortley, *The Theory of Atomic Spectra*, Cambridge University Press, 1963.

[14] W. Low, "Paramagnetic Resonance Spectra of Some Ions in the 3d and 4f Shells in Cubic Crystalline Fields," *Phy. Rev.*, vol. 101, pp. 1827, 1956.

[15] J.E. Wertz, J. W. Orton, and P. Auzins, "Spin Resonance of Point Defects in Magnesium Oxide," *J. Appl. Phys.*, vol. 33, no. 1, pp. 322-328, 1962.

[16] R. S. De Biasi, "Influence of the S^3 Term on the EPR Spectrum of Cr^{3+} in Cubic Symmetry Sites in MgO," *Journal of Magnetic Resonance*, vol. 44, pp. 479-482, 1981.

[17] A. J. Freeman, R. B. Frankel *eds.*, *Hyperfine Interactions*, Academic Press New York, 1967, *c.f.* Ch 1 by B. Bleaney.

[18] Richard Bramley, personal communication

[19] A. Yariv, *Quantum Electronics*, Wiley, 1st ed., 1967.